How to cite: *Angew. Chem. Int. Ed.* **2023,** *62,* e202218078
International Edition: doi.org/10.1002/anie.202218078
German Edition: doi.org/10.1002/ange.202218078

NMR

Determining the Physico-Chemical Composition of Biomolecular Condensates from Spatially-Resolved NMR

*Christian F. Pantoja, Alain Ibáñez de Opakua, Maria-Sol Cima-Omori, and Markus Zweckstetter**

Abstract: Liquid-Liquid phase separation has emerged as fundamental process underlying the formation of biomolecular condensates. Insights into the composition and structure of biomolecular condensates is, however, complicated by their molecular complexity and dynamics. Here, we introduce an improved spatially-resolved NMR experiment that enables quantitative analysis of the physico-chemical composition of multi-component biomolecular condensates in equilibrium and label-free. Application of spatially-resolved NMR to condensates formed by the Alzheimer's disease-associated protein Tau demonstrates decreased water content, exclusion of the molecular crowding agent dextran, presence of a specific chemical environment of the small molecule DSS, and ≈150-fold increased concentration of Tau inside the condensate. The results suggest that spatially-resolved NMR can have a major impact in understanding the composition and physical chemistry of biomolecular condensates.

Biomolecular condensation of proteins and nucleic acids is implicated in a wide range of biological processes and human diseases.[1] Formation of biomolecular condensates in cells is linked to the physico-chemical process of liquid-liquid phase separation (LLPS) of molecular components.[2] Multivalent interactions involving intrinsically disordered proteins (IDPs) and low-complexity domains are often essential in promoting LLPS and biomolecular condensation.[3] Small-molecule therapeutics concentrate in protein condensates affecting drug activity.[4] Small molecule partitioning also affects the formation and properties of biomolecular condensates as demonstrated for adenosine triphosphate.[5] In addition, hydration plays an important role in the formation and regulation of biomolecular condensates.[6]

Due to the molecular complexity and dynamic nature of condensates, effective tools to investigate their composition and structure are required. This is the case for biomolecular condensates in cells, which often contain hundreds of proteins and nucleic acids.[1] Even for biomolecular condensates reconstituted in vitro from a limited number of components, however, it is challenging to obtain accurate component quantification.[7] This is particularly the case for water and other small molecules, which often cannot be labeled to allow their selective observation and thus quantification inside multicomponent condensates. In addition, available approaches for quantification of even single components are often performed under non-equilibrium conditions and thus do not fully capture the dynamic nature of biomolecular condensates. Here, we show that these challenges can be overcome through improved spatially-resolved NMR, providing quantitative insights into the composition of multicomponent condensates in equilibrium and label-free.

To be able to study biomolecular condensates in equilibrium, we phase separated the 441-residue IDP Tau (Figure S1; Table S1) with the molecular crowding agent dextran, centrifuged the sample and formed a macroscopic condensate at the bottom of the NMR tube (Figure 1a, left). In contrast to previous approaches,[8] the Tau condensate does not cover the full length of the NMR tube, but the condensate as well as the dilute phase contribute to the NMR signal. To achieve high sample and temperature stability, we used a coaxial NMR sample setup combining an inner Shigemi tube and an external tube filled with methanol-d_4 for temperature control (Figure 1a left; Figure S2). We then mapped the signal intensity of the water signal along the z-axis by applying a permanent gradient during the NMR acquisition period (Figure S3). For a uniformly mixed, non-phase separated sample, we observed the typical bell-shaped profile that represents the spin density along the z-axis (Figure 1a, right, grey). In the case of the Tau condensate sample, an intensity drop occurred in the region from ≈9–13 mm (Figure 1a, right, black). The intensity drop suggests a reduction of 18.8 ± 0.5 % water content in the protein-rich phase compared to the protein-dilute upper phase (Figure S4).

An additional challenge for spatially-resolved NMR of biomolecular condensates, is the suppression of the water resonance. Highly efficient water suppression is necessary,

[*] C. F. Pantoja, Dr. A. Ibáñez de Opakua, M.-S. Cima-Omori, Prof. Dr. M. Zweckstetter
German Center for Neurodegenerative Diseases (DZNE)
Von-Siebold-Str. 3a, 37075 Göttingen (Germany)
E-mail: Markus.Zweckstetter@dzne.de
Prof. Dr. M. Zweckstetter
Max Planck Institute for Multidisciplinary Sciences
Am Faßberg 11, 37077 Göttingen (Germany)

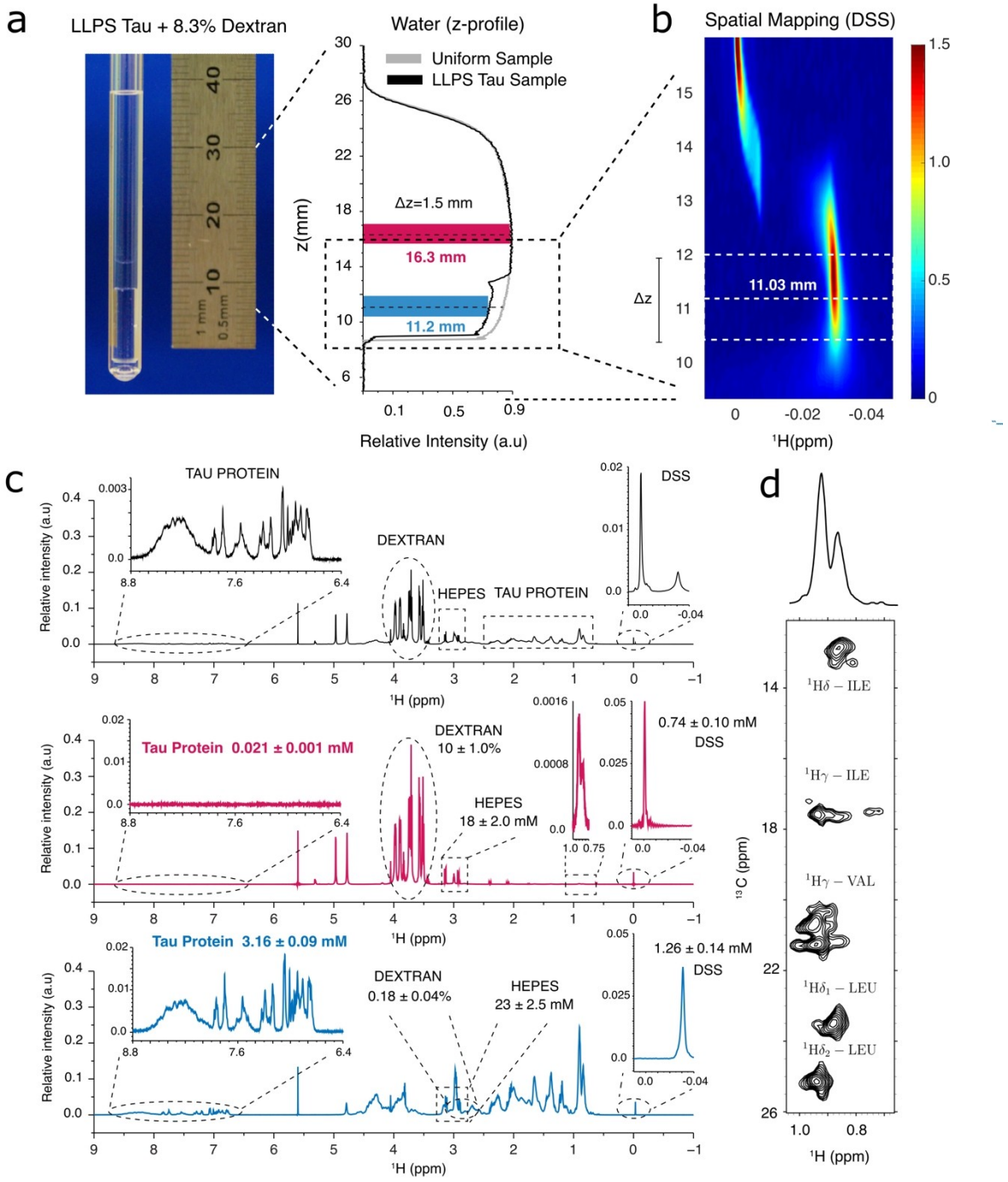

Figure 1. Label-free multi-component quantification of Tau condensates by spatially-resolved NMR spectroscopy. a) Slice-selective detection of NMR spectra of the condensed and dilute protein phase in equilibrium. Tau phase separation was promoted with 8.3% dextran (left). (Right) z-profile experiment monitoring the signal of water along the NMR coil in a uniformly mixed reference sample (grey) and the Tau condensate sample (black). The positions and widths of the gradient-selected slices of the dilute (pink) and condensed phase (blue) are marked. b) DSS signal along the *z*-axis monitored by slice-selective WET-DPFGSE. The ^{1}H chemical shift of DSS in the dilute phase was set to 0 ppm. Signal intensities are color coded from blue to red. c) ^{1}H NMR spectra of the condensed (blue) and dilute phase (pink) recorded with WET-DPFGSE at 25 °C. A standard ^{1}H WET NMR spectrum without slice selection (black) is shown for comparison. Concentrations of the individual components are indicated. d) Non-selective ^{1}H-^{13}C HSQC of the methyl region of the Tau condensate sample. The observed cross peaks arise mostly from the protein-dense lower phase.

in order to be able to quantify the $\approx 10^{5}$–10^{6} lower concentrated protein and small molecule components in the condensate. However, most of the well-known water suppression methods are not compatible with spatial encod-

ing elements. To overcome this limitation, we introduced the water suppression enhanced through T_1 effects (WET) pulse sequence element[9] into the slice-selective Doubled Pulsed Field Gradient Selective Echo (DPFGSE) pulse sequence[10] (Figure S5). The WET block is placed before the slice selection element and avoids saturation of the protein resonances.

We then applied the spatially-resolved WET-DPFGSE NMR pulse sequence to the two-phase condensate sample of Tau. Using a magnetic field gradient together with selective NMR pulses, we selectively detected 1.5 mm thick slices along the *z*-axis of the phase-separated sample (Figure 1a, right). The slice thickness chosen covers a spectral width of 10 ppm ($\Delta\omega \approx 7$ kHz at 700 MHz) ensuring a good compromise between signal-to-noise ratio and spatial selectivity. The two slices were positioned near the center of each phase, where maximum magnetic field homogeneity was present (Figure 1a). This is important, because in phase separated systems magnetic susceptibility changes at the interphase region cause NMR line broadening associated with B_0 inhomogeneities.[11] In addition, non-negligible slice thicknesses require careful positioning of the slices in order to ensure that the acquired NMR signals belong to the desired phase. To further support the selection of the slice positions, we mapped the NMR signal of the reference compound sodium 3-(trimethylsilyl) propane-1-sulfonate (DSS) along the *z*-axis. In a slice of $\approx$1.5 mm, we detected the maximum signal intensity of DSS inside the Tau condensate (Figure 1b).

We then recorded slice-selective, one-dimensional ^{1}H NMR spectra in the condensed lower and the dilute upper phase of the Tau condensate (Figure 1c). In the dilute upper phase, we detected the NMR signals of Tau, dextran, DSS, and 4-(2-hydroxyethyl)-1-piperazineethanesulfonic acid (HEPES). In the condensed lower phase, the NMR signals of Tau, DSS and HEPES were present (Figure 1c). Only very weak signals of dextran were observed in the Tau condensate, indicating that the molecular crowding agent is largely excluded from the condensate (Figure S5). In contrast, the Tau protein was strongly enriched in the condensate (Figure 1c). For quantification (see Methods section), we selected Tau's methyl signals that can provide the most favorable signal-to-noise ratio and retain high mobility even in the condensate (Figure 1c,d; Table S2). The analysis determined the Tau concentration in the dilute and condensed phase as 0.021 ± 0.001 mM and 3.16 ± 0.09 mM, respectively (Figure 1c and S6). The Tau concentration in the condensate is thus 150-fold higher than in the dilute phase.

The improved spatially-resolved NMR experiment also allowed us to quantifiy the concentrations of dextran, DSS and buffer in both phases (Figure 1c and S6; Table S2): 10 ± 1 % and 0.18 ± 0.04 % dextran in the upper and lower phase, respectively; 0.74 ± 0.10 mM and 1.26 ± 0.14 mM DSS, respectively, corresponding to a partition coefficient of 1.7 ± 0.3 in the condensed lower phase; 18.0 ± 1.9 mM and 23.0 ± 2.5 mM HEPES, i.e. a $\approx$30 % enrichment of HEPES in the condensed phase. We further note that the DSS signal is shifted by $\approx$0.03 ppm to lower chemical shift compared to the dilute phase, demonstrating that DSS experiences a distinct chemical environment in the protein-dense lower phase.

Next, we investigated the temperature-dependence of Tau condensation. To this end, we prepared a Tau condensate without crowding agent. Consistent with previous studies,[12] we observed Tau phase separation in a low ionic strength buffer. Supported by centrifugation, two stable phases were formed. The phase-separated sample was then stored at 4 °C for one week to ensure that the system reached equilibrium. The concentrations of Tau in both the condensate and the dilute phase were subsequently quantified using the novel WET-DPFGSE NMR experiment at stepwise increasing temperatures (Figure 2a). Raising the temperature from 5 to 10 °C and from 10 to 15 °C, increased the Tau concentration in the condensed phase by 2.4–7.4 % in each step (Figure 2a; blue lower row). In parallel, the concentration of Tau in the dilute phase was decreased (Figure 2a, red upper row). Increase of the temperature to 20, 25, 30 and 35 °C further increased the Tau concentration in the condensed phase. At 35 °C, the Tau concentration in the condensate was $\approx$46 % higher than at 5 °C (Figure 2a).

Real time monitoring of the Tau concentration during the temperature jump experiment using spatially-resolved NMR, further highlights the importance of reaching equilibrium prior to determining phase diagrams. After raising the temperature by 5 °C, approximately 2 hrs were required before a stable Tau concentration in the condensate was reached (Figure 2b). Even after 5 hrs, the concentration in the dilute phase was still slightly decreasing at temperatures $<$25 °C (Figure 2a, upper row). In addition, the differences between peak height and peak intensity changes in the condensed phase when raising the temperature suggest that chemical exchange processes or temperature-induced sample inhomogeneities contribute to peak broadening and thus affect more strongly the peak height.[13]

Previous studies showed that Tau can experience lower critical solution temperature (LCST) or upper critical solution temperature (UCST) phase separation in a context-dependent manner[14] This assessment has profound implications related to the kinetic process. For systems that undergo LCST, the system is undergoing, after temperature increase, demixing driven by nucleation or spinodal decomposition.[15] Contrary, in systems that display UCST the next equilibrium condition is reached mainly by diffusion. Visual inspection showed that the Tau-rich phase turned turbid when the temperature was raised (Figure S7). This observation is consistent with an entropy-driven nucleation process driven by water in the condensed phase. Nucleation sites rich in water are formed and after fusion are expelled from the protein-rich phase. Consequently, the protein concentration increases along with a "dehydration process" of the lower phase. In the dilute upper phase, no turbidity was visible likely because of less extensive protein nucleation due to the lower Tau concentration.

After reaching constant Tau signal intensities, a z-profile experiment was recorded at each temperature (Figure 2c). The temperature-dependent z-profiles of the water resonance showed that the height of the condensed phase

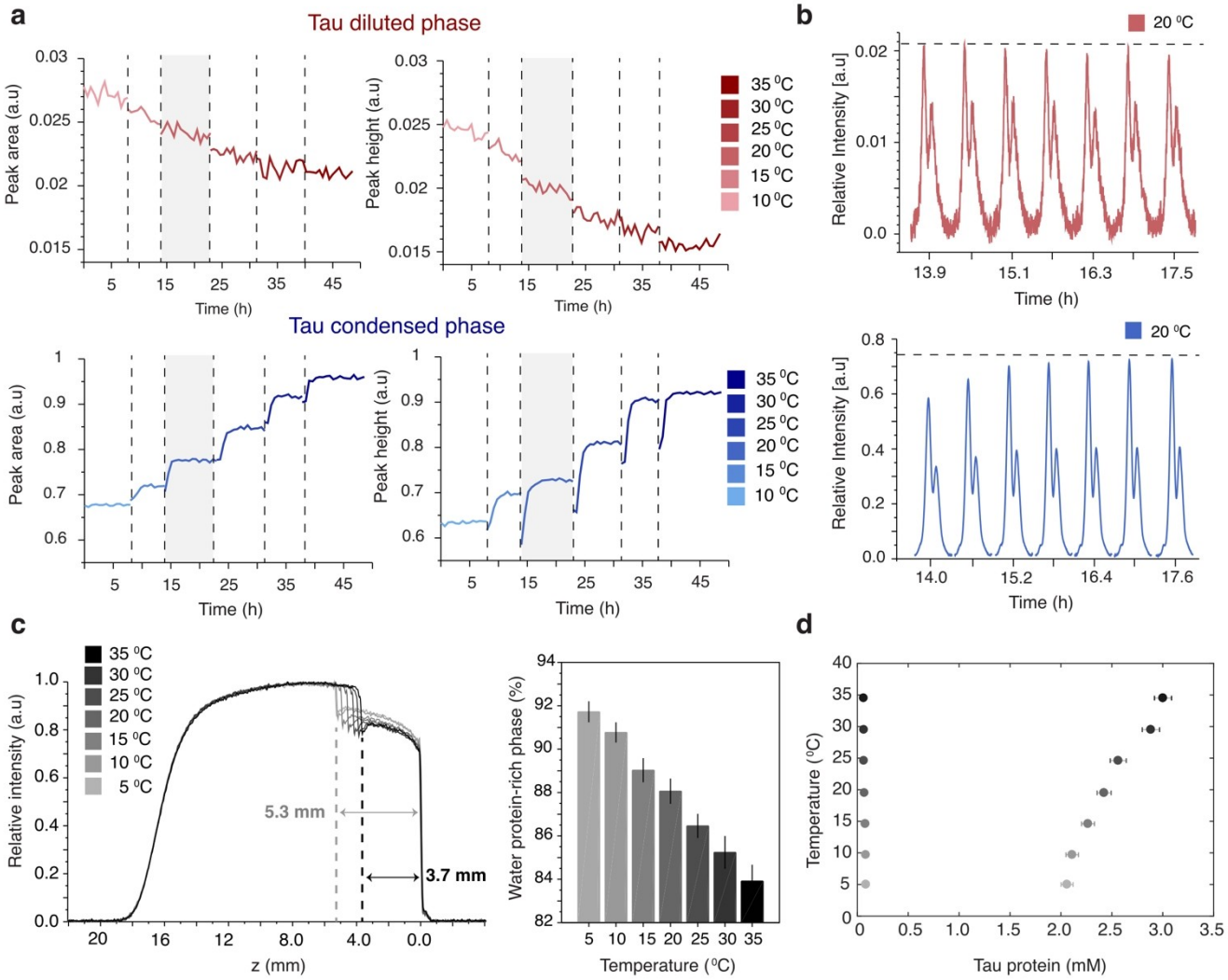

Figure 2. Kinetics of Tau condensation followed by spatially-resolved NMR. a), b) Time-dependent area and height of the methyl signals of Tau in the condensed (blue, lower panels) and dilute (red, upper panels) phase in temperature-jump experiments. The Tau condensate was formed at low ionic strength without dextran. NMR spectra of the two phases were recorded using the slice-selective WET-DPFGSE experiment. Vertical dashed lines mark temperature changes (see legend). b) Time-dependent WET-DPFGSE methyl signals observed after temperature jump from 15 to 20 °C (marked in grey in (a)). Dashed lines indicate near equilibrium condition. c) z-profile experiments recorded after the system reached near equilibrium. (Right) Relative amount of water in the protein-rich phase calculated from the normalized z-profile. d) Phase diagram of Tau determined by spatially-resolved NMR. Tau concentrations in the diluted and condensed phase (at/near equilibrium) determined in the slice-selective NMR spectra are displayed (see also Table S3). Error bars are based on signal-to-noise ratios in the spectra and the uncertainty in the concentration of the reference Tau sample. All NMR spectra were recorded at a 700 MHz NMR spectrometer.

decreased with increasing temperature. At 35 °C, the height was 30 % smaller than at 5 °C (0.3736 ± 0.0002 cm at 35 °C vs 0.5324 ± 0.0002 cm at 5 °C; Figure 2c). Using the information provided by the z-profile experiment, the amount of water in the Tau condensed phase was then estimated. At 5 °C, we observed an 8.28 % decrease in water content in the condensed phase when compared with the dilute phase. At 35 °C, the decrease in water content in the condensed phase reached 16 %. The compaction of the condensed phase thus likely arises from the decrease in water content in the condensed phase with increasing temperature, in agreement with the importance of dehydration for LLPS.[16]

In order to determine the phase diagram of Tau, the areas under the methyl proton signals, which were measured after reaching equilibrium, were converted into Tau concentrations (see Methods section). The Tau concentrations in the condensed and dilute phase represent the high and low concentration part of the phase diagram (Figure 2d). At 5 °C, the Tau molar concentration is ≈32 % lower than at 35 °C ($[Tau]_{35°C}$: 3.0 mM and $[Tau]_{5°C}$: 2.0 mM), in agreement with the percentage of compaction observed by the z-profile experiments (Figure 2c). In parallel, the Tau concentration in the dilute phase was decreased by ≈26 % in the studied temperature range (Figure 2c).

We showed that improved spatially-resolved NMR enables the quantification of multiple components in biomolecular condensates in equilibrium and label-free. Protein, small molecules and water can be simultaneously quantified with high reliability in both the condensed and dilute phase. Multi-component quantification can be performed in a temperature-dependent manner in real time providing insight into the kinetics of condensation processes. The improved WET-DPFGSE NMR experiment thus complements and extends previous NMR approaches that relied on the use of fluorinated molecules for quantification of protein or small molecule concentrations in phase-separated systems.[13,17] In addition, Raman microscopy can be useful to quantify protein concentrations, on the basis of the signals emerging from the different amounts of water present in the condensed and dilute phase.[18]

The improved spatially-resolved NMR is applicable to effectively any IDP as long as its NMR resonances are observable. Protein concentrations determined by spatially-resolved NMR characterize protein phase diagrams with high reliability. This will be important to better understand the mechanisms that drive the phase separation of IDPs and their modulation by disease-associated mutations and post-translational modifications. The high reliability of phase diagrams determined by spatially-resolved NMR will also be important to improve current computational methods which explore the molecular forces that govern biomolecular phase transitions.[19] We further expect that the ability to simultaneously observe proteins, small molecules and water will provide critical guidance in understanding the partitioning into and modulation of biomolecular condensates by small molecules. Importantly, spatially resolved NMR is not restricted to the simultaneous quantification of the concentration of proteins, small molecules and water in phase separated systems, but is also sensitive to differences in the chemical environment in the two phases.

Acknowledgements

C.F.P. acknowledges the Deutscher Akademischer Austauschdienst (DAAD) for the Research Grants Doctoral program in Germany, 2019/20 (personal ref. no. 91726791). M.Z. was supported by the European Research Council (ERC) under the EU Horizon 2020 research and innovation program (grant agreement no. 787679). Open Access funding enabled and organized by Projekt DEAL.

Conflict of Interest

The authors declare no conflict of interest.

Data Availability Statement

The data that support the findings of this study are available in the Supporting Information of this article.

Keywords: Biomolecular condensates · Spatially-resolved NMR · Multicomponent quantification · Phase diagram · Tau protein

[1] a) S. F. Banani, H. O. Lee, A. A. Hyman, M. K. Rosen, *Nat. Rev. Mol. Cell Biol.* **2017**, *18*, 285–298; b) S. Alberti, A. A. Hyman, *Nat. Rev. Mol. Cell Biol.* **2021**, *22*, 196–213.

[2] A. A. Hyman, C. A. Weber, F. Jülicher, *Annu. Rev. Cell Dev. Biol.* **2014**, *30*, 39–58.

[3] J. M. Choi, A. S. Holehouse, R. V. Pappu, *Annu. Rev. Biophys.* **2020**, *49*, 107–133.

[4] I. A. Klein, A. Boija, L. K. Afeyan, S. W. Hawken, M. Fan, A. Dall'Agnese, O. Oksuz, J. E. Henninger, K. Shrinivas, B. R. Sabari, I. Sagi, V. E. Clark, J. M. Platt, M. Kar, P. M. McCall, A. V. Zamudio, J. C. Manteiga, E. L. Coffey, C. H. Li, N. M. Hannett, Y. E. Guo, T. M. Decker, T. I. Lee, T. Zhang, J. K. Weng, D. J. Taatjes, A. Chakraborty, P. A. Sharp, Y. T. Chang, A. A. Hyman, N. S. Gray, R. A. Young, *Science* **2020**, *368*, 1386–1392.

[5] a) A. Patel, L. Malinovska, S. Saha, J. Wang, S. Alberti, Y. Krishnan, A. A. Hyman, *Science* **2017**, *356*, 753–756; b) N. A. Yewdall, A. A. M. Andre, M. H. I. van Haren, F. H. T. Nelissen, A. Jonker, E. Spruijt, *Biophys. J.* **2022**, *121*, 3962–3974.

[6] a) Y. Dorone, S. Boeynaems, E. Flores, B. Jin, S. Hateley, F. Bossi, E. Lazarus, J. G. Pennington, E. Michiels, M. De Decker, K. Vints, P. Baatsen, G. W. Bassel, M. S. Otegui, A. S. Holehouse, M. Exposito-Alonso, S. Sukenik, A. D. Gitler, S. Y. Rhee, *Cell* **2021**, *184*, 4284–4298; b) J. Ahlers, E. M. Adams, V. Bader, S. Pezzotti, K. F. Winklhofer, J. Tatzelt, M. Havenith, *Biophys. J.* **2021**, *120*, 1266–1275.

[7] a) A. V. Ceballos, C. J. McDonald, S. Elbaum-Garfinkle, *Methods Enzymol.* **2018**, *611*, 31–50; b) N. M. Milkovic, T. Mittag, *Methods Mol. Biol.* **2020**, *2141*, 685–702; c) G. A. Mountain, C. D. Keating, *Methods Enzymol.* **2021**, *646*, 115–142; d) A. Bremer, A. E. Posey, M. B. Borgia, W. M. Borcherds, M. Farag, R. V. Pappu, T. Mittag, *Biomol. Eng.* **2022**, *12*, 1480.

[8] a) A. C. Murthy, N. L. Fawzi, *J. Biol. Chem.* **2020**, *295*, 2375–2384; b) L. E. Wong, T. H. Kim, D. R. Muhandiram, J. D. Forman-Kay, L. E. Kay, *J. Am. Chem. Soc.* **2020**, *142*, 2471–2489; c) B. E. Ackermann, G. T. Debelouchina, *Angew. Chem. Int. Ed.* **2019**, *58*, 6300–6305; *Angew. Chem.* **2019**, *131*, 6366–6371; d) J. C. Fuentes-Monteverde, S. Becker, N. Rezaei-Ghaleh, *Protein Sci.* **2021**, *30*, 1315–1325; e) A. C. Murthy, G. L. Dignon, Y. Kan, G. H. Zerze, S. H. Parekh, J. Mittal, N. L. Fawzi, *Nat. Struct. Mol. Biol.* **2019**, *26*, 637–648; f) J. P. Brady, P. J. Farber, A. Sekhar, Y. H. Lin, R. Huang, A. Bah, T. J. Nott, H. S. Chan, A. J. Baldwin, J. D. Forman-Kay, L. E. Kay, *Proc. Natl. Acad. Sci. USA* **2017**, *114*, E8194–E8203.

[9] a) R. J. Ogg, P. B. Kingsley, J. S. Taylor, *J. Magn. Reson. Ser. B* **1994**, *104*, 1–10; b) S. H. Smallcombe, S. L. Patt, P. A. Keifer, *J. Magn. Reson. Ser. A* **1995**, *117*, 295–303.

[10] a) W. Kozminski, *Pol. J. Chem.* **2000**, *74*, 1185–1189; b) K. Stott, J. Stonehouse, J. Keeler, T.-L. Hwang, A. J. Shaka, *J. Am. Chem. Soc.* **1995**, *117*, 4199–4200; c) J. N. Dumez, *Prog. Nucl. Magn. Reson. Spectrosc.* **2018**, *109*, 101–134.

[11] B. T. Martin, G. C. Chingas, O. M. McDougal, *J. Magn. Reson.* **2012**, *218*, 147–152.

[12] T. Ukmar-Godec, S. Hutten, M. P. Grieshop, N. Rezaei-Ghaleh, M. S. Cima-Omori, J. Biernat, E. Mandelkow, J. Soding, D. Dormann, M. Zweckstetter, *Nat. Commun.* **2019**, *10*, 2909.

[13] a) C. F. Pantoja, M. Zweckstetter, N. Rezaei-Ghaleh, *Phys. Chem. Chem. Phys.* **2022**, *24*, 6169–6175; b) J. E. Bramham, A. P. Golovanov, *Nat. Commun.* **2022**, *13*, 1767.

[14] a) Y. Lin, J. McCarty, J. N. Rauch, K. T. Delaney, K. S. Kosik, G. H. Fredrickson, J. E. Shea, S. Han, *eLife* **2019**, *8*, e42571; b) S. Najafi, Y. Lin, A. P. Longhini, X. Zhang, K. T. Delaney, K. S. Kosik, G. H. Fredrickson, J. E. Shea, S. Han, *Protein Sci.* **2021**, *30*, 1393–1407; c) S. K. Rai, A. Savastano, P. Singh, S. Mukhopadhyay, M. Zweckstetter, *Protein Sci.* **2021**, *30*, 1294–1314.
[15] K. Binder, *Rep. Prog. Phys.* **1987**, *50*, 783–859.
[16] S. Park, R. Barnes, Y. Lin, B.-j. Jeon, S. Najafi, K. T. Delaney, G. H. Fredrickson, J. E. Shea, D. S. Hwang, S. Han, *Commun. Chem.* **2020**, *3*, 83.
[17] J. Niu, C. Qiu, N. L. Abbott, S. H. Gellman, *J. Am. Chem. Soc.* **2022**, *144*, 10386–10395.
[18] K. Yokosawa, S. Kajimoto, D. Shibata, K. Kuroi, T. Konno, T. Nakabayashi, *J. Phys. Chem. Lett.* **2022**, *13*, 5692–5697.
[19] a) Y.-H. Lin, J. Song, J. D. Forman-Kay, H. S. Chan, *J. Mol. Liq.* **2017**, *228*, 176–193; b) J. McCarty, K. T. Delaney, S. P. O. Danielsen, G. H. Fredrickson, J.-E. Shea, *J. Phys. Chem. Lett.* **2019**, *10*, 1644–1652; c) X. Zeng, A. S. Holehouse, A. Chilkoti, T. Mittag, R. V. Pappu, *Biophys. J.* **2020**, *119*, 402–418.

Manuscript received: December 7, 2022
Accepted manuscript online: February 27, 2023
Version of record online: March 15, 2023